IEEE Photonics Journal
An IEEE Photonics Society Publication

Open Access

Dual-Function Metal–Insulator–Metal Plasmonic Optical Filter

Volume 7, Number 1, February 2015

Tae-Woo Lee
Da Eun Lee
Soon-Hong Kwon

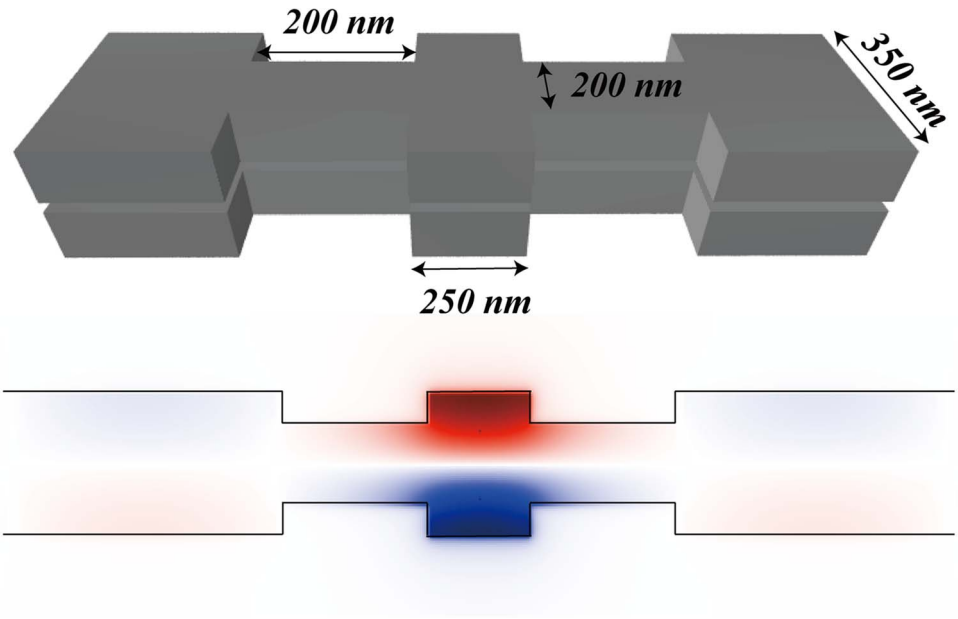

DOI: 10.1109/JPHOT.2014.2387254
1943-0655

IEEE photonics SOCIETY

IEEE

Dual-Function Metal–Insulator–Metal Plasmonic Optical Filter

Tae-Woo Lee, Da Eun Lee, and Soon-Hong Kwon

Department of Physics, Chung-Ang University, Seoul 156-756, Korea

DOI: 10.1109/JPHOT.2014.2387254

Manuscript received November 18, 2014; revised December 9, 2014; accepted December 11, 2014. Date of publication January 13, 2015; date of current version January 27, 2015. This work was supported in part by the National Research Foundation of Korea (NRF) grant funded by the Korean government (MSIP) under Grant NRF-2013R1A2A2A01014491 and in part by the Chung-Ang University Research Scholarship Grants in 2013. Corresponding author: S.-H. Kwon (e-mail: soonhong.kwon@gmail.com).

Abstract: We suggest a dual-function plasmonic optical filter based on a metal–insulator–metal waveguide that has a deep subwavelength air gap 10 nm in thickness and a waveguide width of 350 nm. Because the dispersion curves of even and odd waveguide modes have different dependences on the waveguide width, and only the odd mode has a cutoff frequency, the proposed structure can have dual functionality, acting as a resonant tunneling filter for odd modes and a simple waveguide for even modes.

Index Terms: Plasmonics, nanocavities.

1. Introduction

Miniaturization of photonic devices is essential to developing more compact photonic integrated circuits. Plasmonic structures play key roles in the realization of ultracompact photonic devices because they can confine of light beyond the diffraction limit [1], [2]. Recent studies have introduced various types of plasmonic structure with deep subwavelength light confinement, such as plasmonic cavities [3], [4], waveguides [5]–[8], and optical filters [9], [10], which would be essential building blocks in photonic circuits. Among many types of plasmonic structures, metal–insulator–metal (MIM) plasmonic waveguides have received much attention for use in compact photonic devices because MIM waveguides can localize light in the deep subwavelength cross-sectional area in the insulator between metals [8], [11], [12].

On the other hand, to realize more compact photonic integrated circuits in which multiple photonic components are arranged, multifunctional devices should be developed to reduce the complexity of the circuit. Recently, non-periodic metallic grooves [13] and photonic crystal waveguides [14] have been demonstrated to show multiple functionalities in reasonable designs determined using numerical parameter searches.

In this paper, we proposed a dual-function optical filter consisting of an MIM cavity and waveguides based on the mode symmetry and dispersion properties. In an MIM waveguide, the dispersion curves of even and odd modes have different dependences on the waveguide width, and only odd modes have a cutoff frequency, which results in forbidden frequency regions in propagation of the waveguide mode. By combining these properties of the two waveguide modes, the proposed filter performs two different roles for even and odd waveguide modes. Even waveguide modes can be transmitted with high transmittance $(T > 75\%)$ for a broad spectral range

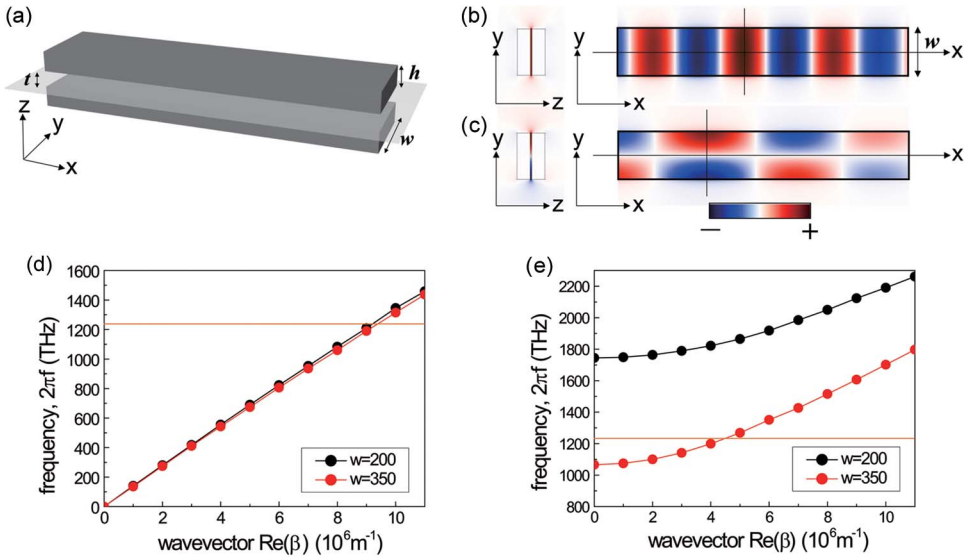

Fig. 1. (a) Schematic diagram of an MIM waveguide. Two metal strips (dark gray boxes) are made of silver. Vertical electric field (E_z) mode profiles of top and side views of (b) even waveguide mode and (c) odd waveguide mode with a wavelength of 1550 nm in a waveguide having a width w of 350 nm. Top-view mode profiles are obtained from the center of the MIM waveguide [gray plane in (a)]. Dispersion curves of (d) even mode and (e) odd mode for waveguide widths of 200 nm (black) and 350 nm (red). Horizontal orange lines represent the wavelength of $\lambda = 1550$ nm ($2\pi f = 1215$ THz).

(1200–1750 mm); in contrast, relatively high transmittance ($T > 49\%$) of odd modes is allowed only for a narrow spectral range corresponding to the plasmonic cavity resonance with a wavelength of 1547 nm and a linewidth at full width at half-maximum ($\Delta\lambda_{\mathrm{FWHM}}$) of 105 nm.

2. MIM Plasmonic Waveguide and Dispersion Properties

Fig. 1(a) shows a schematic diagram of an MIM waveguide consisting of two silver strips with a deep subwavelength air gap. Each silver strip has a thickness (h) of 100 nm and a waveguide width (w) of 200 or 350 nm. The air gap size (t) is 10 nm, which is 150 times smaller than the wavelength of 1550 nm. In this waveguide, two types of waveguide modes exist depending on the symmetry of the modes. Fig. 1(b) shows side and top views of the dominant electric field (E_z) profiles of a waveguide mode that has even mirror symmetry with respect to the center of the waveguide (x axis). In contrast, Fig. 1(c) shows electric field profiles of a waveguide mode with odd mirror symmetry. In these figures, the excited waveguide modes were calculated for a wavelength of 1550 nm in waveguides with a width of 350 nm. According to the symmetry, the waveguide modes in Fig. 1(b) and (c) are called even and odd waveguide modes, respectively. In both waveguide modes, the electric fields are strongly localized in the deep subwavelength air gap between the silver strips because of effective index guiding, even though there is no physical boundary in the horizontal direction. Both waveguide modes are transverse magnetic field (TM) modes, as dominant electric field is z-direction.

To understand the propagation characteristics of both waveguide modes, we obtained the dispersion curves of the even and odd modes for waveguide widths of 200 and 350 nm, as shown in Fig. 1(d) and (e). The frequency of the even waveguide mode is linearly proportional to the wave vector, and the even mode is allowed in the entire frequency range [see Fig. 1(d)]. When the waveguide width increases from 200 to 350 nm, the dispersion curve shifts slightly to shorter frequencies. This is because the effective index of the waveguide increases slightly. However, the effect of the waveguide width on the dispersion curve is relatively small as the waveguide width changes from 200 to 350 nm.

In contrast with that of the even mode, the dispersion curve for the odd mode has a strong width dependence. The electric field maximum of the odd mode is located at the edge of the waveguide in Fig. 1(c). Therefore, changing the waveguide width affects the dispersion curve significantly. Furthermore, the odd mode has a cutoff frequency (cutoff wavelength) at zero wave vector, which is the lowest allowed frequency (longest wavelength) that can be propagated by the waveguide. Propagation of waveguide modes with a frequency below the cutoff frequency is forbidden. As shown in Fig. 1(e), the dispersion curve moves considerably upward as the width of the waveguide is adjusted from 350 to 200 nm, with a large jump in the cutoff frequency. As a result, the waveguide with a width of 200 nm has a higher cutoff frequency ($2\pi f =$ 1744 THz) than the waveguide with a width of 350 nm (1066 THz), and the allowed frequency in the waveguide moves toward frequencies above the cutoff frequency. For example, for the odd waveguide mode with a frequency of 1215 THz (wavelength of 1550 nm), because the frequency is higher than the cutoff frequency of the wider waveguide ($w = 350$ nm) and lower than that of the narrower waveguide ($w = 200$ nm), propagation is allowed along the wider waveguide but forbidden along the narrower waveguide. Therefore, the narrow waveguide can work as a mirror for the odd mode with a wavelength of 1550 nm.

In this paper, the waveguide mode, cavity mode, and transmission are calculated by the 3-D finite-difference time-domain (FDTD) method. Silver is represented by the Drude model based on the experimentally determined dielectric functions [4], [15], [16]. The real part (ε_r) and imaginary part (ε_i) of the dielectric function are described as follows:

$$\varepsilon_r(\omega) = \varepsilon_\infty - \frac{\omega_p^2}{\omega^2 + \gamma^2}, \quad \varepsilon_i(\omega) = \frac{\gamma\omega_p^2}{\omega(\omega^2 + \gamma^2)}$$

where the background dielectric constant (ε_∞), plasma frequency (ω_p), and damping factor (γ) are set to 3.14, 9.13 eV, and 0.0210 eV, respectively. The background material is set to air. To describe the 10 nm air gap size accurately in the simulations, the grid sizes in the x, y, and z directions are set to 5, 5, and 1 nm, respectively.

3. Structure of Dual-Function Optical Filter

On the basis of the dispersion properties of the even and odd modes, we propose a dual-function waveguide filter with two waveguide widths of 200 nm and 350 nm, as shown in Fig. 2(a). A cavity region with a width of 350 nm and a length (L_c) of 250 nm is sandwiched between two mirror regions consisting of narrow waveguides ($w = 200$ nm) with a length (L_m) of 400 nm and input/output wide waveguides ($w = 350$ nm) sequentially. Along the waveguide axis (x axis), the change in the waveguide width causes spatial variation in the cutoff frequency of the odd mode [see Fig. 2(b)]. Because the widths of the cavity and the input/output waveguides are set to 350 nm, their cutoff frequency (cutoff wavelength) is 1066 THz (1767 nm). On the other hand, the mirror waveguide width of 200 nm has a cutoff frequency (cutoff wavelength) of 1744 THz (1080 nm). The odd mode can propagate along the waveguide only if the odd waveguide mode has a higher frequency than the cutoff frequency. Therefore, a photonic well having a frequency ranging from 1066 to 1744 THz can be built in the cavity region. When the odd mode is excited in the cavity region with a frequency lower than the cutoff frequency of the mirror region, the mode would be localized by the mirror waveguide owing to cutoff frequency difference. In fact, a resonant mode with a resonant wavelength of 1547 nm, indicated by the orange line in Fig. 2(b), is strongly localized in the cavity region, as shown in the electric field profile in Fig. 2(c). On the other hand, the cavity mode can be transmitted into the input/output wide waveguides by photon tunneling over the forbidden mirror region with finite length because the wavelength of the cavity resonance is also placed in the allowed region of the input/output waveguide [see Fig. 2(b)]. The mode profile indicates that the cavity mode originates in the odd waveguide mode of Fig. 1(c). To excite the cavity mode, an electric dipole source with z-axis polarization is placed at the antinode of the mode profile.

To understand the loss properties of the proposed structure, we investigate the Q factors (Q_tot, Q_cavity, Q_wg, and Q_abs) as functions of the mirror waveguide length (L_m). The Q factor is

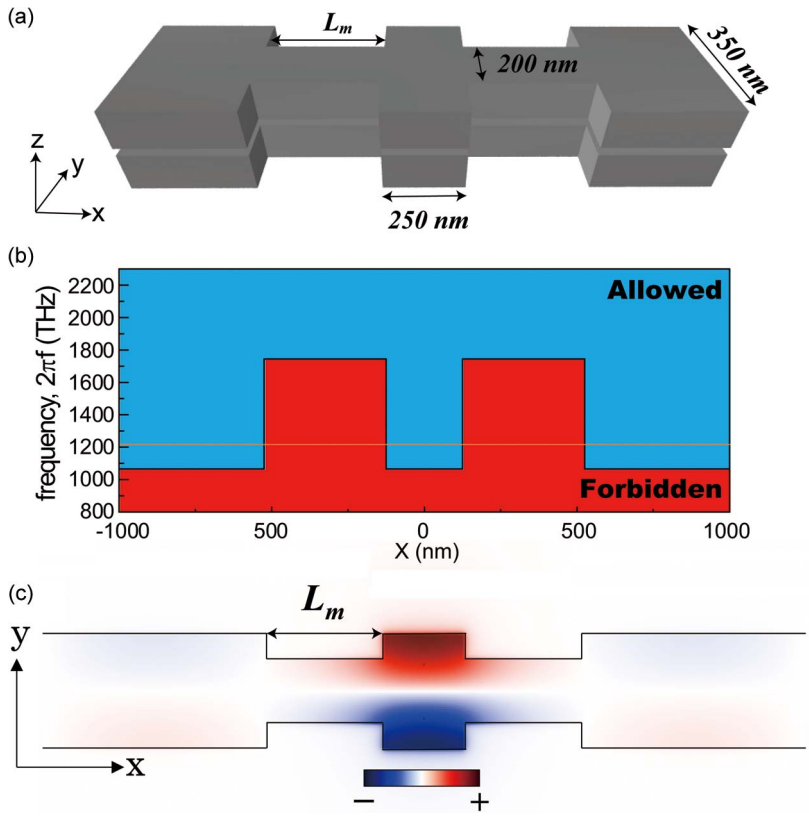

Fig. 2. (a) Schematic of proposed dual-mode waveguide filter. L_m indicates length of mirror waveguide. (b) Cutoff frequency of the odd mode as a function of the waveguide width modulation along the waveguide axis (x axis). The frequency region above the cutoff frequency corresponds to the allowed region for odd mode propagation. Orange line represents the resonant wavelength of 1547 nm ($2\pi f = 1218$ THz). (c) Vertical electric field (E_z) profile of the odd mode at the center of the air gap. L_m is 400 nm.

defined as follows: $2\pi f \times (\textit{stored energy in cavity}/\textit{power loss})$ [17]. The total loss of the proposed structure consists of the cavity radiation loss, waveguide loss, and metallic absorption loss. Because the Q factor is inversely proportional to the loss, we can calculate Q_{tot}, Q_{cavity}, Q_{wg}, and Q_{abs} by calculating the respective losses. In the cavity, horizontal leakage into free space due to weak index guiding causes the cavity radiation loss, and the metallic absorption loss arises from power attenuation in the metal by ohmic loss. On the other hand, the waveguide loss corresponds to the coupling loss between the cavity mode and the input/output waveguides. We calculate each loss as follows. First, Q_{tot} is obtained from the time decay of the cavity total energy. Next, we calculate $Q_{optical}$, which is the total loss in a structure that has no metallic absorption loss. $Q_{optical}$ can be computed as the damping factor in the Drude model goes to zero [4], [18], which gives the value of Q_{abs} from the equation $1/Q_{total} = (1/Q_{optical}) + (1/Q_{absorption})$. Further, we calculate the cavity loss and waveguide loss by summing the Poynting vectors over the surface covering the cavity and the cross-sectional surface of the input/output waveguide, respectively. Using the ratio between the cavity loss and the waveguide loss, Q_{cavity} and Q_{wg} are directly obtained by the following equation: $1/Q_{optical} = (1/Q_{cavity}) + (1/Q_{waveguide})$.

As shown in Fig. 3, the total Q factor increases following Q_{cavity} as L_m increases and becomes saturated at a value of 35 when L_m exceeds 350 nm because the dominant losses, the cavity radiation loss, and metallic absorption loss, remain the same, as indicated by the constant Q_{cavity} and Q_{abs}. Because the metallic absorption loss is determined by the amount of cavity energy inside the metal, and the mode profile is not changed, Q_{abs} has an almost constant value of 89 for different values of L_m. Q_{cavity}, which is affected mainly by the air gap size because the effective

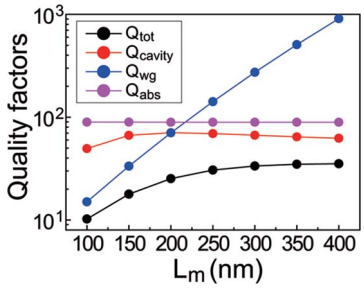

Fig. 3. Quality factors of the odd cavity mode in the proposed structure as a function of mirror length (L_m). Q_{tot} (black), Q_{cavity} (red), Q_{wg} (blue), and Q_{abs} (purple) are inversely proportional to the total loss, cavity radiation loss, waveguide loss, and metallic absorption loss, respectively.

index of the mode determines the horizontal leakage [4], [16], has an almost constant value of 68 for cutoff mirror lengths greater than 150 nm. On the other hand, the coupled energy from the cavity to the input/output wide waveguide decreases with increasing mirror length because the mirror effect becomes stronger. Therefore, Q_{wg} increases exponentially as the mirror length increases. Q_{wg} is estimated to be 15 for $L_m = 100$ nm and increases to 910 for $L_m = 400$ nm. In Fig. 3, the waveguide coupling loss is dominant for L_m shorter than 200 nm; thus, Q_{tot} decreases according to the dependence of Q_{wg} on the mirror length. For a high waveguide coupling ratio, a smaller L_m is required; however, for a high Q_{cavity} or narrow operating linewidth, an L_m value larger than 200 nm should be chosen. The dominant cavity loss is mainly from y directional radiation and can be suppressed by applying multipole-cancellation mechanism [19] of higher order cavity mode, resulting in the increase of Q_{cavity}. Q_{abs} can be increased by introducing high index material in the middle of air gap [20]. By increasing Q_{cavity} and Q_{abs}, the overall Q factor would be increased.

4. Transmission Characteristics of Even and Odd Waveguide Modes

The proposed structure acts as a resonant cavity for the odd waveguide mode owing to the cutoff frequency difference between the waveguides with different widths (see Fig. 2). However, because the even waveguide mode has almost the same dispersion curve for different waveguide widths [see Fig. 1(d)], the modulation of the waveguide widths may not affect the propagation of the even mode. To investigate the transmittance properties for the even and odd modes in the broadband wavelength region ranging from 1200 nm to 1750 nm at the input (left) wide waveguide, the transmitted signals in the output (right) wide waveguide are measured, and the wavelength dependences are calculated.

Fig. 4(a) shows high transmittance ($> 75\%$) of the even mode in a broad wavelength region of 1200–1750 nm. A wavelengths of less than 1500 nm, the transmittance is even larger than 90%, and for wavelengths larger than 1500 nm, the transmittance decreases but is still larger than 75%. If monochromatic light with a wavelength of 1547 nm, the cavity resonance of the odd mode, is injected from the input waveguide, 91% transmittance is expected from Fig. 4(a). In fact, Fig. 4(b) shows high transmission of the even mode with a wavelength of 1547 nm from the input waveguide to the output waveguide through the proposed structure. A strong electric field amplitude in the output waveguide, which is comparable with that in the input waveguide, is clearly observed, and the ratio between the field intensity in the input/output waveguides is matched to the transmittance curve of Fig. 4(a). In the even mode, the narrow waveguide ($w = 200$ nm) is not a mirror waveguide but just a simple waveguide. Therefore, because propagation of the even mode is allowed at all frequencies (wavelengths), regardless of the waveguide width, the proposed structure acts as a simple waveguide for the even mode despite the existence of width modulation. In addition, the transmission curve remains almost unchanged even if L_m is changed.

In contrast to even mode transmission, which occurs with large transmittance over a broad spectral range in the proposed structure, odd mode transmission is allowed only for a narrow

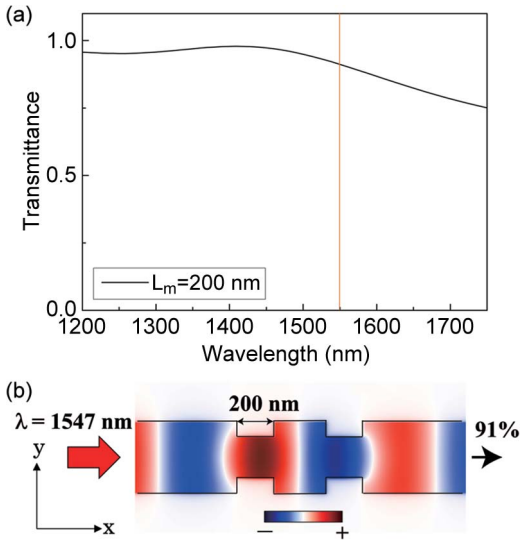

Fig. 4. (a) Transmission curve of the even mode for the proposed structure with mirror length $L_m = 200$ nm. Vertical orange line indicates the odd mode cavity resonance wavelength of 1547 nm. (b) Vertical electric field (E_z) profile of even waveguide mode transmission. Red arrow represents the injection of monochromatic light with a wavelength of 1547 nm. The proposed structure transmits 91% of the injected light.

wavelength range corresponding to the cavity resonance. We investigate the transmission curves of the odd waveguide mode for mirror lengths (L_m) of 100, 200, and 300 nm. At transmission peak is observed at the cavity resonant wavelengths, which are estimated to be 1530, 1547, and 1550 nm for $L_m = 100$, 200, and 300 nm, respectively. As L_m decreases and the mirror effect of the narrow waveguide becomes weaker, a larger transmittance is obtained at resonance. When L_m is 100 nm, the transmittance is calculated as 87% at resonance, and the peak has a broad linewidth at full width at half-maximum $(\Delta\lambda_{FWHM})$ of 250 nm. For $L_m = 300$ nm, the transmittance is only 20% at resonance, however, with a relatively narrow linewidth of 75 nm. The trade-off between transmission and bandwidth is determined by modulating the mirror length. Fig. 5(b) and (c) show the dominant E_z profiles of the odd mode transmission on resonance (1547 nm) and off resonance (1300 nm), which are indicated by the red and blue lines, respectively, in Fig. 5(a) in the structure with a mirror length of 200 nm. The transmission peak has a $\Delta\lambda_{FWHM}$ of 105 nm. For on resonance transmission, the transmittance has a relatively high value of 49%. On the other hand, the off resonance transmission is negligibly small $(T = 5\%)$. Therefore, the proposed structure with $L_m = 200$ nm allows the propagation of the odd mode only in the wavelength range of 1495–1600 nm. Transmittance through the photonic well is considered as photonic resonant tunneling, which can be understood by similar way with quantum tunneling effect. Therefore, the transmittance through the mirror region decreases exponentially with increasing the mirror length, L_m [21]. If Q_{cavity} and Q_{abs} are increased by manipulating mode shape and introducing high index material inside air gap, Q_{tot} will saturate at the higher Q values, which suggests higher transmission with similar Q for same L_m with the proposed structure.

5. Conclusion

In summary, we theoretically proposed a dual-function MIM plasmonic optical filter consisting of a cavity region and two mirrors with different waveguide widths. Because only the odd mode has a cutoff frequency, and the frequency depends on the waveguide width, light with a wavelength (λ) of 1547 nm, which has an odd cavity mode profile, can be confined in a cavity region with a size of $350 \times 250 \times 10$ nm$^3 = 0.00024\lambda^3$. The odd waveguide mode shows resonant tunneling for a cavity resonance with a peak wavelength of 1547 nm and a linewidth of 105 nm.

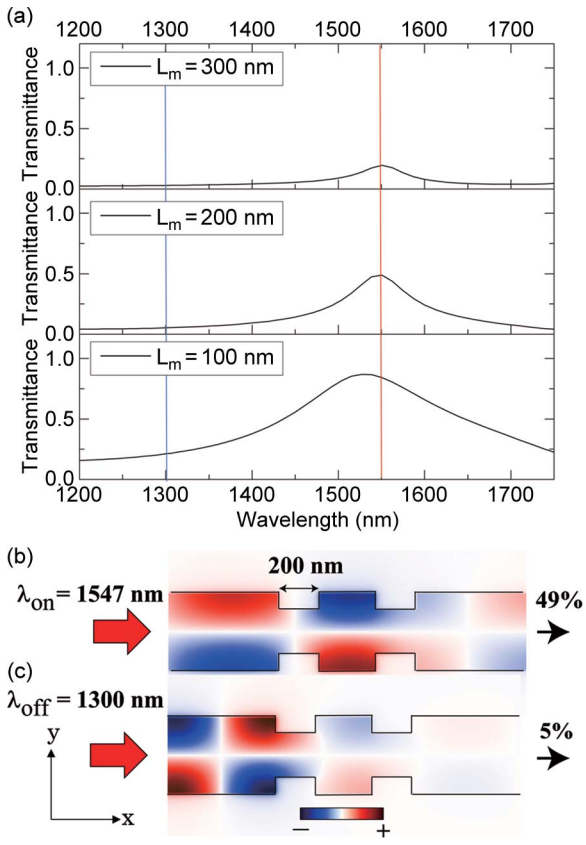

Fig. 5. (a) Transmission curves of the odd mode for L_m values of 300, 200, and 100 nm, from top to bottom. Dominant E_z field profiles of the odd mode transmission (b) on resonance and (c) off resonance. Red arrows indicate injection of monochromatic light with a wavelength of 1547 nm [on resonance: red line in (a)] and 1300 nm [off resonance: blue line in (a)].

Because the dispersion curve of the even mode does not depend on the waveguide width, the even mode can transmit more than 75% in a broad spectral range of 1200–1750 nm for the proposed structure with waveguide width modulation. By using simple width modulation and the cutoff frequency of the odd mode, the proposed structure functions simultaneously as both a resonant optical filter with a narrow spectral range and a simple waveguide with high transmittance for a broad spectral range, where the functionality is determined simply by the symmetry of the injected waveguide mode. This proposed submicrometer-sized photonic device, which allows the spectral transmittance to be selected by varying two different parameters, will facilitate the construction of more compact photonic integrated circuits. The dual function filter can be fabricated by depositing metal over thin dielectric layer on the metal substrate, defining the structure through the e-beam lithography and dry-etching, and removing the thin dielectric layer by wet etching. If active material is embedded in the cavity region, nano-laser or optical switching devices are also constructed.

References

[1] D. K. Gramotnev and S. I. Bozhevolnyi, "Plasmonics beyond the diffraction limit," *Nature Photon.*, vol. 4, no. 2, pp. 83–91, Jan. 2010.
[2] W. L. Barnes, A. Dereux, and T. W. Ebbesen, "Surface plasmon subwavelength optics," *Nature*, vol. 424, pp. 824–830, Aug. 2003.
[3] B. Min *et al.*, "High-Q surface-plasmon-polariton whispering-gallery microcavity," *Nature*, vol. 457, pp. 455–458, Jan. 2009.
[4] S.-H. Kwon, "Plasmonic ruler with angstrom distance resolution based on double metal blocks," *IEEE Photon. Technol. Lett.*, vol. 25, no. 16, pp. 1619–1622, Aug. 2013.

[5] S. I. Bozhevolnyi, V. S. Volkov, E. Devaux, J.-Y. Laluet, and T. W. Ebbesen "Channel plasmon subwavelength waveguide components including interferometers and ring resonators," *Nature*, vol. 440, pp. 508–511, Mar. 2006.
[6] J. Grandidier *et al.*, "Gain-assisted propagation in a plasmonic waveguide at telecom wavelength," *Nano Lett.*, vol. 9, no. 8, pp. 2935–2939, Aug. 2009.
[7] A. Pannipitiya, I. D. Rukhlenko, M. Premaratne, H. T. Hattori, and G. P. Agrawal, "Improved transmission model for metal–dielectric–metal plasmonic waveguides with stub structure," *Opt. Exp.*, vol. 18, no. 6, pp. 6191–6204. Mar. 2010.
[8] G. Veroins and S. Fan, "Modes of subwavelength plasmonic slot waveguides," *J. Lightw. Technol.*, vol. 25, no. 9, pp. 2511–2521, Sep. 2007.
[9] Q. Zhang, X.-G. Huang, X.-S. Lin, J. Tao, and X.-P. Jin, "A subwavelength coupler-type MIM optical filter," *Opt. Exp.*, vol. 17, no. 9, pp. 7549–7555, Apr. 2009.
[10] X. S. Lin and X.-G. Huang, "Tooth-shaped plasmonic waveguide filters with nanometeric sizes," *Opt. Lett.*, vol. 33, no.23, pp. 2874–2876, Dec. 2008.
[11] J. A. Dionne, L. A. Sweatlock, and H. A. Atwater, "Plasmon slot waveguides: Towards chip-scale propagation with subwavelength-scale localization," *Phys. Rev. B*, vol. 73, no. 3, Jan. 2006, Art. ID. 035407.
[12] P. Neutens, P. Van. Dorpe, L. de Vlaminck, L. Lagae, and G. Borghs, "Electrical detection of confined gap plasmons in metal–insulator–metal waveguides," *Nature Photon.*, vol. 3, pp. 283–286, May 2009.
[13] J. Wang, C. Hu, and J. Zhang, "Multifunctional and multi-output plasmonic meta-elements for integrated optical circuits," *Opt. Exp.*, vol. 22, no. 19, pp. 22 753–22 762, Sep. 2014.
[14] N. Saidani, W. Belhadj, and F. AbdelMalek, "Novel all-optical logic gates based photonic crystal waveguide using self imaging phenomena," *Opt. Quantum Electron.*, DOI: 10.1007/11082-014-0047-4, 2014.
[15] P. B. Johnson and R. W. Chrity, "Optical constants of the novel metals," *Phys. Rev. B*, vol. 6, no. 12, pp. 4370–4379, Dec. 1972.
[16] S.-H. Kwon, "Deep subwavelength-scale metal–insulator–metal plasmonic disk cavities for refractive index sensors," *IEEE Photon. J.*, vol. 5, no. 1, Feb. 2013, Art. ID. 4800107.
[17] M. C. Teich and B. E. A. Saleh, *Fundamentals of Photonics*. Mississauga, ON, Canada: Wiley, 1991.
[18] S.-H. Kwon, "Ultrasmall plasmonic cavity for chemical sensing," *Plasmonics*, vol. 8, no. 2, pp. 963–967, Jun. 2013.
[19] S. G. Johnson, S. Fan, and J. D. Joannopoulos, "Multipole-cancellation mechanism for high-Q cavities in the absence of a complete photonic band gap," *Appl. Phys. Lett.*, vol. 78, no. 22, pp. 3388–3390, 2001.
[20] R. F. Oulton, V. J. Sorger, D. A. Genov, D. F. P. Pile, and X. Zhang, "A hybrid plasmonic waveguide for subwavelength confinement and long-range propagation," *Nature Photon.*, vol. 2, pp. 496–500, 2008.
[21] B. S. Song, T. Asano, and S. Noda, "Physical origin of the small modal volume of ultra-high-Q photonic double-heterostructure nanocavities," *New J. Phys.*, vol. 8, no. 9, p. 209, Sep. 2006.